

An electromagnetic wearable 3-DoF resonance human body motion energy harvester using ferrofluid as a lubricant

Shuai Wu^{1,2,3}, P. C. Luk³, Chunfang Li¹, Xiangyu Zhao¹, and Zongxia Jiao^{1,2}

1. School of Automation Science and Electrical Engineering, Beihang University, Beijing, 100191, China

2. Science and Technology on Aircraft Control Laboratory, Beihang University, Beijing, 100191, China

3. Electrical Power and Drives Group, Power Engineering Centre, Cranfield University, Cranfield, MK43 0AL, U.K

Abstract

Wearable Energy harvester offers clean and continuous power for wearable sensors or devices, which can play an important role in the health monitoring, motion track and so on. In this study, we investigated a small electromagnetic resonance wearable kinetic energy harvester. A permanent magnet (PM) which was tied with two springs is forming a 3-degree-of-freedom (3-DoF) vibrator and is put in a box. Ferrofluid was adopted which is adsorbed at the pole of PM and makes the PM away from the surface of the box which decreased the friction significantly. Coils are placed on the outside surface and the electric energy is generated when the PM is vibration. It can be used to harvest kinetic energy of human and offer continuous power. The effect of ferrofluid was simulated and analyzed which indicated that the ferrofluid can keep the PM contactless even under 10 times gravity acceleration. A prototype was developed and tested under different loading conditions. Resistance load experiments results indicated that the proposed harvester can generate 0.75mW average power when walking and 1.4mW when running. An energy storage circuit which can transfer the generated alternating power to 5V direct current was developed to store the electrical power into capacitor. Energy storage experiments results indicated that the average storage power when walking and running are 20.8 μ W and 35.2 μ W, respectively. The developed harvester can be placed on the shoe and used to offer continuous

Preprint submitted to Applied Energy

December 24, 2016

power supply for wearable sensor and device.

Keywords:

Energy harvester, wearable, electromagnetic, generator, ferrofluid

1. Introduction

Wearable sensors are developing fast and increasingly used widely resulting in an increase in the demand of independent power supplies. Since the progress of battery technologies is still very progressive and its power density is relative low, which makes wearable devices bulky and heavy, along with the inconvenience of frequent recharge [1].

An alternative approach is using wearable generator to extract energy from the environment to produce continuous electrical power to extend the charging interval or as the main power supply. The energy from human body represents a feasible source for wearable devices. Indeed, the human body is very flexible in generating applicable power from sources of heat dissipation, joint rotation, enforcement of body weight, vertical displacement of mass centers, as well as elastic deformation of tissues and other attachments. The average adult consumes approximately 2000kcal per day, and the power is about 100W. This power is expended during everyday activities, including motions of walking, arm swinging, finger motion, and breathing [1, 2]. A summary of the potential power sources are provided in Fig. 1. In fact, the human body contains enormous amount of energy, the average adult has as much energy stored in fat as a one-ton battery since the energy density of fat is 100 times bigger than current most advanced battery. This opens up opportunities for harvesting energy to power wearable devices. Therefore, wearable energy harvester is expected to play a very important role in powering future wearable devices.

The harvesting energy from human motion has attracted increasing attention in the past decade. Several concepts of wearable energy harvesters based on different mechanisms have been studied, such as piezoelectric [4, 5, 6, 7, 8, 9, 10], thermo-electric [11, 12], nano triboelectric [13], electrostatic [14], and electromagnetic [15, 16, 17]. Article [2] gives a comprehensive review of MEMS-based human energy harvester. In these approaches, electromagnetic harvesters convert multitudinous mechanical energy to electrical energy flexibly. Harvesting vibration energy can be achieved by induction [18, 19], by magnetic spring vibrator [20], or even by multi-frequencies vibration struc-

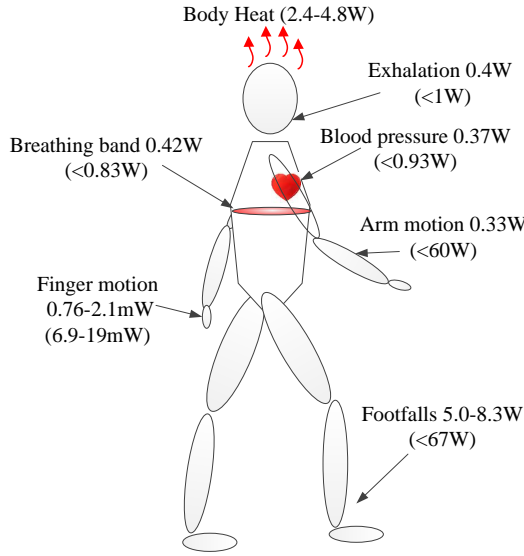


Figure 1: Possible power recovery from human body [3]

ture [21]. Rolling magnet inside some coils for harvesting energy from human locomotion is demonstrated in [22, 23]. Here, this work also focuses on electromagnetic energy harvesters.

However, the performance of electromagnetic energy scavenging devices is limited by many inherent congenital factors. Most of existing human powered electromagnetic energy harvesting devices are designed on the principle of linear resonance where an inertial mass is mounted on a spring damper and is excited at the resonance frequency of human motion. This approach presents numerous drawbacks, two of the most important are that the human motion is a combination of low frequency vibrations and the linear harvester resonant peak is very narrow. Low frequency vibration has low power. Thus, the device only can generate very little power and will even worse when body vibration frequency deviates from the resonance. To overcome these difficulties, a new 3-Dof resonant kinetic energy harvester is proposed in this paper. This harvester places a PM in a rectangle box which connects to two borders with two elastic strings and working as a vibrator. Two windings are placed on the outer surface which generate electrical power when the PM vibrate in the box. The first innovation of this energy harvester is the PM has 3-DoF motion (two dimensional planar motion and one rotation motion) with different resonant frequency which can absorb human motion energy

more efficiently. The second is that ferrofluid is introduced which make the PM frictionless which reduce the energy loss significantly. The mathematics model of the proposed energy harvester is studied and the design parameters are optimized. A prototype of the harvester and a energy harvester circuit which transfer the generated alternate current power to direct current power and store into capacitor or battery are fabricated and tested. The experiment results indicated that the average energy harvesting capability is over $30\mu\text{W}$. The results demonstrate that the harvester can be integrated with shoe and serves as a wearable power supply for low power wearable devices.

2. Human Energy Analysis and Harvester Design

2.1. Human Energy Analysis

In inertial harvesters, the output power is maximized when the harvester resonant frequency is matched to the motion frequency. Therefore, characterizing the properties of the harvested power requires an in-depth study of human motion (e.g., the frequencies associated with different motions) and human mobility patterns [24]. Previous studies of examined energy of particular human motions [24, 25] indicate that human motion is a combination of low frequency vibrations ($\leq 10\text{Hz}$), the dominant motion frequency range is $1.1 - 3.8\text{Hz}$. The main challenge for a resonant energy harvester is that low frequency vibration contains low energy. That why human powered resonant inertial energy harvester usually cannot generate big power. In order to increase energy harvesting power, high frequency resonance is expected. But for human body, the foot fall can be regarded as a impact, which contains high frequency power. In present study we design a resonant energy harvester to absorb the impact energy of foot fall which contains high frequencies energy.

2.2. Harvester Design

The proposed 3-DoF human body motion energy harvester is shown in Fig. 2. It has a rectangle box contain a PM inside which is magnetized in the direction of up surface of box. The PM is connected by two elastic springs, which make the PM has 3-DoFs, which are move along the spring direction, move along with the vertical direction of spring and rotation in the box surfing. All of these 3-DoFs have resonance frequencies which should match to the frequency ranges of human motion in different directions. Therefore, the stiffness of the springs is the key design parameters. It is easy to know,

the stiffness along the string direction is higher than the vertical direction of string in this design. Hence the harvester will be put on the side of the shoe and let the elastic string along the footfall direction which can absorb the high frequency impact energy, and the vertical direction resonant will absorb the moving energy of foot.

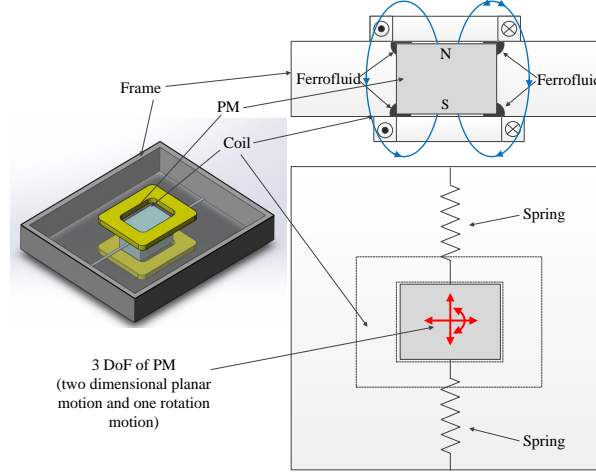


Figure 2: Structure of proposed harvester

The friction force is also a big challenge for improving efficiency of this type of small electro-magnetic energy harvester.

Ferrofluids are suspensions of small ferromagnetic particles in a base fluid. It is a fluid which can be attracted by magnetic field, thus it can offer some interesting characteristics in electro-magnetic harvester. An electromagnetic energy harvester that uses an array of rectangular permanent magnets as a spring-less proof mass and ferrofluid as a lubricating material has been studied in [26, 17]. In [15], the ferrofluid in a tank is used to harvest vibratory energy by conforming to different shapes.

In order to reduce the friction between the resonator and the box, some ferrofluid is added on the PM. The ferrofluid will along the edge of the poles and makes the PM float away from the wall of the container which makes the PM frictionless. It is very helpful for increasing the energy harvest efficiency.

3. Modeling and simulation

3.1. Modeling of resonance

The geometry definition diagram is shown in Fig. 3. The center of PM position is denoted as (x, y) . The left spring anchor point is denoted as (x_a, x_b) , and the right spring anchor point is denoted as (x_a, x_b) . The rotary angle of PM is denoted as θ .

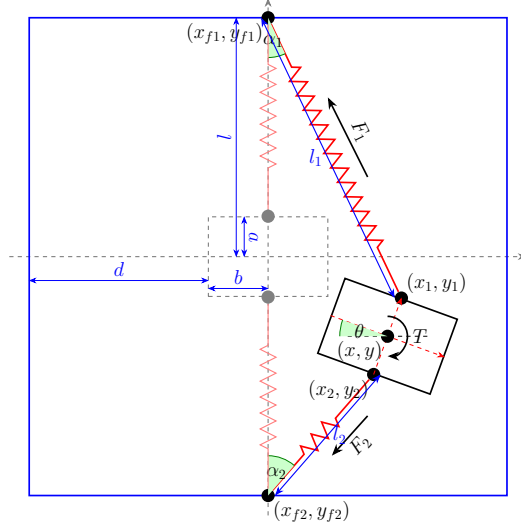


Figure 3: Geometry definition diagram

The anchor positions can be calculated by:

$$\begin{aligned} x_1 &= x - a \cos \theta \\ y_1 &= y + a \sin \theta \end{aligned} \quad (1)$$

$$\begin{aligned} x_2 &= x + a \cos \theta \\ y_2 &= y - a \sin \theta \end{aligned} \quad (2)$$

The length of the spring can be calculated by:

$$\begin{aligned} l_1 &= \sqrt{(x_1 - x_{f1})^2 + (y_1 - y_{f1})^2} \\ &= \sqrt{(x_1 + (l + a))^2 + y_1^2} \\ l_2 &= \sqrt{(x_2 - x_{f2})^2 + (y_2 - y_{f2})^2} \\ &= \sqrt{(x_2 - (l + a))^2 + y_2^2} \end{aligned} \quad (3)$$

115 where l is the initial length of spring when the PM in the balance position.
 116 The spring tension force equals to:

$$\begin{aligned} F_1 &= \begin{cases} K_s(l_1 - l_0) & \text{IF } l_1 - l_0 > 0 \\ 0 & \text{ELSE} \end{cases} \\ F_2 &= \begin{cases} K_s(l_2 - l_0) & \text{IF } l_2 - l_0 > 0 \\ 0 & \text{ELSE} \end{cases} \end{aligned} \quad (4)$$

117 where K_s is the stiffness of the spring, l_0 is the unextended length of spring.
 118 The force on the X -direction equals:

$$F_x = -(F_1 \sin \alpha_1 + F_2 \sin \alpha_2) \quad (5)$$

119 The force on the Y -direction equals:

$$F_y = F_1 \cos \alpha_1 - F_2 \cos \alpha_2 \quad (6)$$

120 The torque on the PM equals:

$$T = (F_2 \sin \alpha_2 \cos \theta - F_1 \sin \alpha_1 \cos \theta - F_2 \cos \alpha_2 \sin \theta - F_1 \cos \alpha_1 \sin \theta)a \quad (7)$$

121 The most important parameter of the proposed harvester is the resonant
 122 frequency. The resonant frequency is defined as $\sqrt{K_s/m}$ in translation sys-
 123 tem and $\sqrt{K_t/J}$ in rotation system. There are three resonant frequency for
 124 the proposed 3-Dof inertia harvester, e.g., $F_x = \sqrt{K_x/m}$ in X direction trans-
 125 lation Dof, $F_y = \sqrt{K_y/m}$ in Y direction translation Dof, and $F_r = \sqrt{K_r/J}$
 126 of rotational Dof, where K_x , K_y and K_r are stiffness in X , Y and rotational
 127 direction, respectively.

128 For the proposed design, the stiffness in 3 Dof is varying with position
 129 and rotation angle rather than a constant. The stiffness in the X -direction
 130 can be defined as

$$K_x(x, y, \theta) = \frac{(F(x + dx, y, \theta) - F(x, y, \theta))}{dx} \quad (8)$$

131 In a similar way, the stiffness in the Y direction and rotational direction
 132 equal

$$K_y(x, y, \theta) = \frac{(F(x, y + dy, \theta) - F(x, y, \theta))}{dy} \quad (9)$$

133 and

$$K_r(x, y, \theta) = \frac{(T(x, y, \theta + d\theta) - T(x, y, \theta))}{d\theta} \quad (10)$$

134 These equations above indicate that the stiffnesses are function of K_s ,
135 (x, y) , a , l , and l_0 . Therefore, the stiffness can be adjusted by selecting
136 properly parameter to obtain desired values. Especially the l_0 influence sig-
137 nificantly to the stiffness.

138 Based on the definition of three stiffnesses, the resonant frequency in
139 the X , Y and rotation direction can be defined as $\sqrt{K_x/m}$, $\sqrt{K_y/m}$ and
140 $\sqrt{K_r/J}$. The resonant frequency can be obtained by numerical computation
141 method. Letting $l = 15\text{mm}$, $a = 5\text{mm}$, $\theta = 0^\circ$, the normalized resonant
142 frequencies when $l_0 = 8\text{mm}$ and $l_0 = 13\text{mm}$ are shown in Fig 4.

143 The comparison of Fig. 4a and Fig. 4c or Fig. 4b and Fig. 4d indicate
144 that the resonant frequency in the X -axis direction is smaller than the Y -axis
145 direction. For the tension condition ($l_0 = 13\text{mm}$), the resonant frequency in
146 X direction is only about 2/3 in Y -direction. And for the loose condition
147 ($l_0 = 13\text{mm}$), the resonant frequency in X direction is only about 1/2 in
148 Y -direction. Therefore, the X -direction and Y -direction can absorb different
149 frequent energy.

150 The comparison of results of tension condition $l_0 = 13\text{mm}$ and $l_0 = 8\text{mm}$
151 indicate that the more spring extension at neutral position, the higher the
152 resonant frequency. These two figures also show that if the length of string
153 is bigger than l_0 , the resonant frequency is decided by two strings, and if
154 the length of the string is shorter than the l_0 , which means one string is
155 totally loose, the resonant frequency is decided by one string. Therefore, the
156 resonant frequency changes rapidly when one string is loose.

157 The rotation angle of PM (θ) also influence the resonant frequency. Let-
158 ting $l_0 = 14\text{mm}$, the resonant frequencies for X , Y and rotation directions
159 when $\theta = 0^\circ$ and $\theta = 30^\circ$ are shown in Fig. 5. The results illustrate that
160 the rotation angle of PM increase the resonant frequency a little bit beside
161 rotate the resonant frequency contour plot.

162 3.2. Simulation of ferro-fluid effect

163 The friction is a big challenge for a small inertia energy harvester. The
164 ferro-fluid is introduced to reduce the friction by the effect of pushing PM
165 away from the plate which makes the PM contact-less. This is a very intrigu-
166 ing effect which can reduce power loss and increase velocity of PM which re-
167 ally helpful for this kind small energy harvester. This effect can be explained

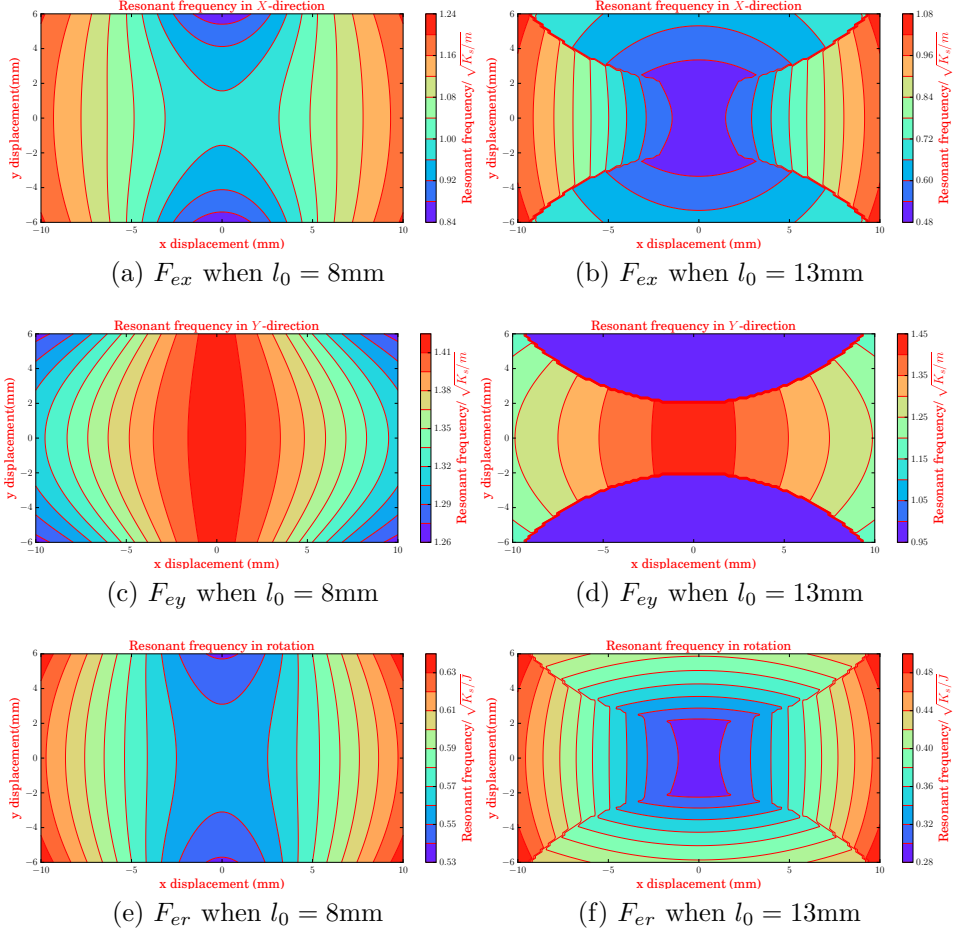


Figure 4: Resonant frequencies for different spring extension conditions

by the magnetization characteristics of ferro-fluids. When assuming ferro-fluids are stable and consist of non-interacting, identical magnetic dipoles, the magnetization curve can be accurately described by the non-dimensional Langevin function for paramagnetic behavior [27, 28]:

$$L(\alpha) = \frac{M}{M_s} = \coth(\alpha) - \frac{1}{\alpha} \quad (11)$$

with the Langevin parameter

$$\alpha = \frac{\mu_0 m_d H}{kT} \quad (12)$$

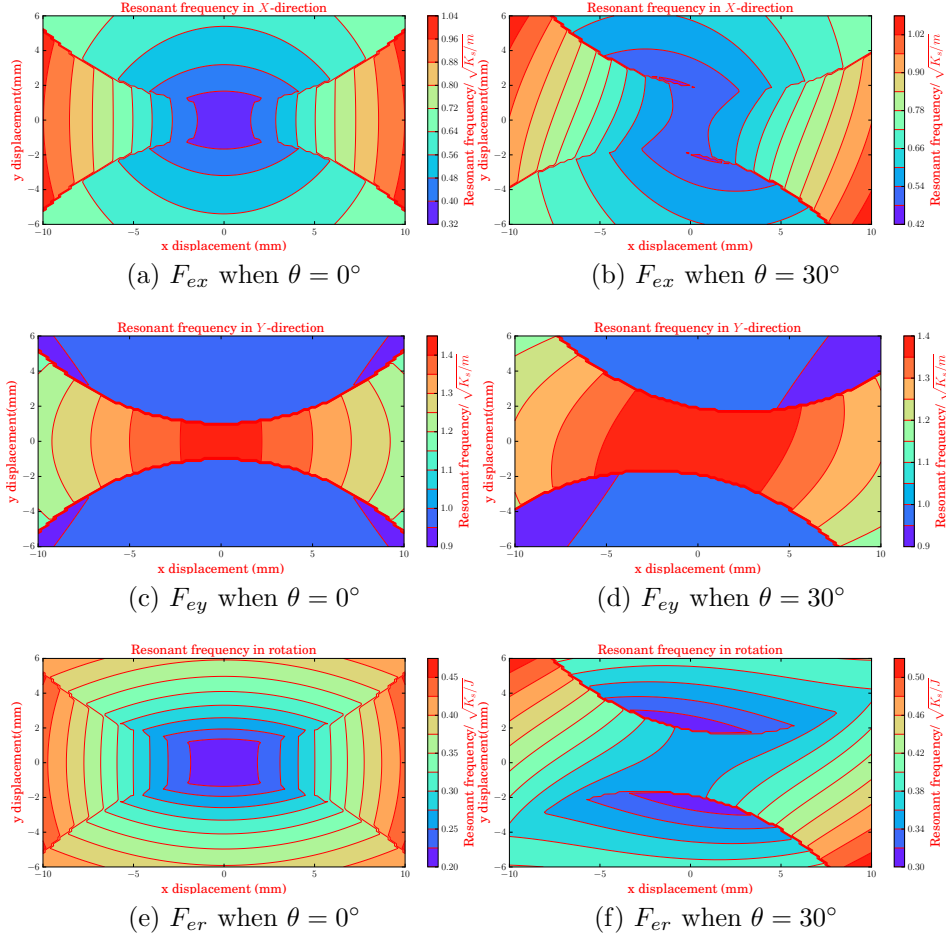


Figure 5: Resonant frequencies for different rotation angles

173 in which $k = 1.18 \cdot 10^{-23} [\text{J/K}]$ is the Boltzmann constant, T is the absolute
 174 temperature and m_d is the magnetic dipole moment. For spheric particles,
 175 m_d is given by

$$m_d = M_d V_d = \frac{1}{6} M_d \pi d^3 \quad (13)$$

176 where M_d is the domain magnetization, which is the saturation magnetiza-
 177 tion of the particle material, V_d and d are volume and diameter of magnetite
 178 particles, respectively. Because the particles are part of the fluid, the satu-
 179 ration magnetization of ferrofluid should product the volume density factor

180 of the domain magnetization.

$$\mathbf{M}_s = \phi_p \mathbf{M}_d \quad (14)$$

181 where M_s is the saturation magnetization of ferrofluid, ϕ_p is the volume
182 fraction of particles in the fluid. The magnetization \mathbf{M} is:

$$\mathbf{M}(\mathbf{H}) = \mathbf{M}_s \quad (15)$$

183 Referring to the reported literatures [29, 27] and the manual(EFH1 [30]),
184 the adopted ferro-fluid contains magnetite particles with an average size of
185 14nm, its magnetite $M_{d,Fe_3O_4} \approx 450\text{kA/m}$, and the $\phi_p = 0.08$. The magneti-
186 zation curve of Eq. (11) is shown in Fig. 6a. There are saturation asymptotes
187 at $M = \pm M_s$ when the absolute value of α increase. The relative permeabil-
188 ity versus magnetic density can be calculated from this curve and it is shown
189 in Fig. 6b. These curves have been experimentally confirmed in [29] and the
190 initial relative permeability value conforms to the document of EFH1 [30, 31].

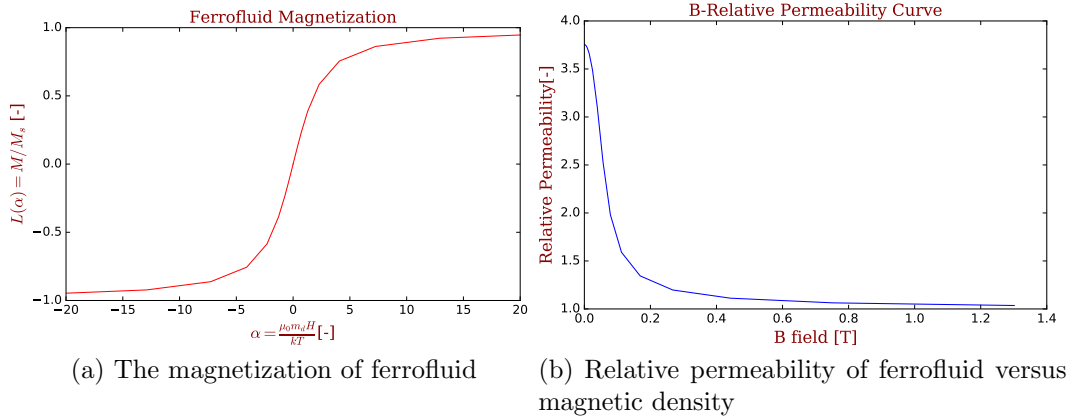


Figure 6: Magnetic characteristics of ferrofluid

191 Substitute $H = 30\text{kA/m}$ and $T = 300\text{K}$ into Eq. (12) can get $L(\alpha) = 0.85$.
192 It is also can be seen that the initial relative permeability is about 3.7 and it
193 is close to 1 when B is over $0.1T$. Therefore, it is reasonable to assume the
194 entire fluid is always fully saturated since the H of PM is much bigger than
195 30kA/m .
196

197 Using an energy balance, article [32] showed that the pressure outside
 198 and inside of a stationary ferrofluid is given by:

$$P(x, y, z) - P_0 = \rho g(z_0 - z) + \mu_0 \int_C M(H) \Delta H dr + \lambda P \quad (16)$$

199 where the 1st term on the right-hand side is the hydrostatic pressure by the
 200 gravity, the 2nd term is the magnetically induced pressure and the 3rd term
 201 is the pressure different across the interface due to surface tension. When
 202 the gravity and surface effects can be neglected, the pressure equation can
 203 be presented as:

$$P(x, y, z) - P_0 = \mu_0 M_s (H(x, y, z) - H_0) \quad (17)$$

204 The Eq.17 shows that for a constant P_0 at the interface, the fluid should have
 205 $H = H_0$. So, the ferro-fluid in a uniform pressure will align with the isometric
 206 of magnetic field strength (iso- H) lines and preferring higher gradients of H .
 Therefore, ferro-fluid will concentrate at the edges, as the Fig. 8 shows.

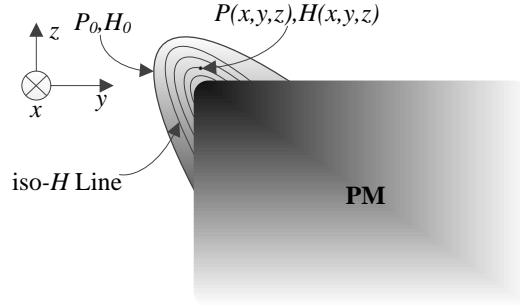


Figure 7: The pressure on the surface and inside of ferro-fluid. The lines indicate equal value of H , which are called iso- H lines. The ferro-fluid will align with iso- H lines in a uniform pressure.

207
 208 If a plate limits the ferro-fluid align with the iso- H line then the pressure
 209 will not equal on the contacting surface which is shown in Fig.9. The push
 210 away force can be calculated by integrating the pressure at the contacting
 211 surface A . When using the above equations to calculate pull-back force, the
 212 difficult parts are in obtain the geometry shape of ferro-fluid and determining
 213 the magnetically intensity distribution in the ferrofluid. Obtain the analytic
 214 model is very difficult, the finite element method (FEM) modeling approach
 215 is a feasible solution [33, 34].

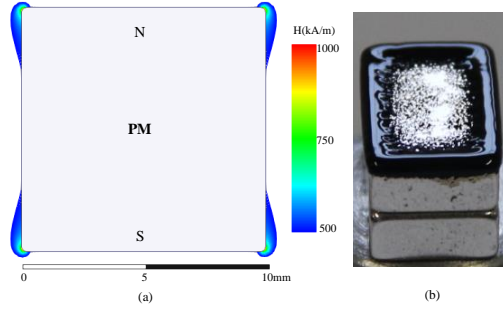


Figure 8: Ferro fluid on a PM will concentrate on the edges, where the magnetizing field gradient is highest. (a) Modeled iso- H line by finite element method (FEM) method, (b) A photograph of ferrofluids on PM.

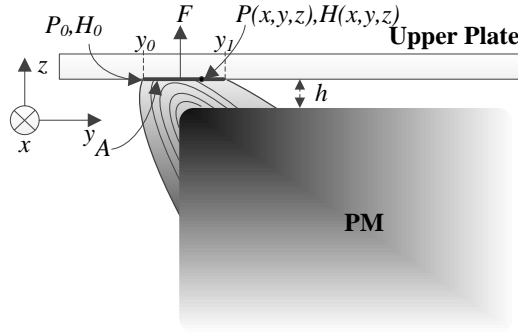


Figure 9: The push away force can be calculated by integrating the pressure at the contacting surface A .

216 Because the profile in direction x is approximately constant. So the push-
217 ing away force per meter can be calculated by

$$\bar{F} = \int_{y_0}^{y_1} P(y, z) dy, \quad \text{at } z = h. \quad (18)$$

218 The total push away force is thus

$$F = \int_0^L \bar{F} = 2(a + b)\bar{F}, \quad (19)$$

219 where $L = 4(a + b)$ is the length of the ferrofluid align the edge.

220 The actual shape of the ferrofluid is difficult to modeling and it deforms
221 when the PM moving in Z -direction, resulting in changed pressure distribu-
222 tion. Therefore, only a predefined shape of ferrofluid is simulated to obtain

223 a proximate result. This is only to validate the pushing sway force can over-
 224 come the gravity and the acceleration force in Z -direction, the accuracy is
 225 acceptable. The radius at the edge of the PM turned out be an important
 226 factor in determining H . It was measured to be $R = 0.2\text{mm}$. Simplified the
 227 the shape of the ferrofluid is a circle with the diameter is $2r = 1\text{mm}$, and the
 228 center is localing at the peaks of the PM with the offset of $t = 0.1\text{mm}$. The
 229 defined model for FEM is shown in Fig.10.

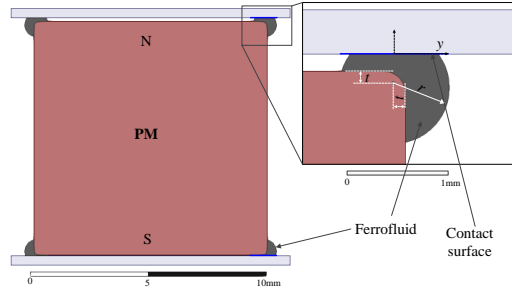


Figure 10: The 2D FEM model to calculate the pressure distribution in ferrofluid.

230 When the PM locals at the center of the two plate, the magnetic induced
 231 pressure on the contact surface of ferrofluid and upper and lower plates will
 232 balance. If the PM offset from the center position in the Z direction, the
 233 magnetic induced pressure at narrow side will increase and the other side will
 234 decrease. Then the PM will be pushed back to the center point in the Z -
 235 direction. This is why the ferro-fluid makes the PM contact-less and reduce
 236 friction. Assume the PM offset to $z = -0.05\text{mm}$, the magnetic field strength
 237 and pressure distribution on the contact surface of ferrofluid and upper and
 238 lower plate is shown in Fig. 11. Integrating the differential pressure with
 239 the contact surface area, it can be calculated that the total push away force
 240 about 0.12N . The mass of the PM is about 15g , therefore, the push away
 241 force is nearly 8 times than the weight when $z = -0.05\text{mm}$. This force will
 242 push the PM back to center position and keep it contact-less even subject
 243 with several times gravity acceleration in Z -direction. This is very useful for
 244 proposed energy harvester.

245 4. Experiments

246 4.1. Prototype and test rig

247 The prototype of proposed generator is shown in Fig. 12. The size of the
 248 moving PM is $10 \times 15 \times 10\text{mm}$, and its mass is 15g . The PM is put in a

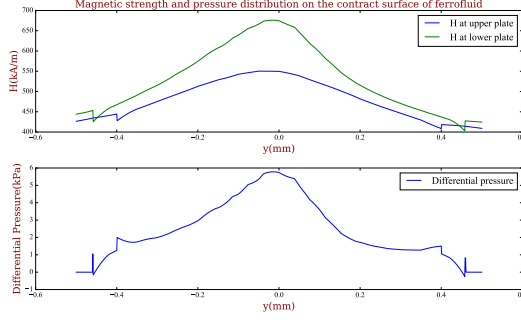


Figure 11: Magnetic field strength and pressure distribution on the contact surface of the ferrofluid when $z = -0.05\text{mm}$.

rectangle container which made by Aluminum and its size is $46 \times 51 \times 10\text{mm}$. Two coils are placed on each of upper and lower plates and the size of each coil is $a = 3\text{mm}$, $t = 2.5\text{mm}$. Then the total thickness of the generator including the two coils is 16mm . The electrical parameters of the two coils include: each coil is about 100 turns; the resistance of each coil is 0.98Ω ; two coils are serially connected thus the total internal resistance is 1.96Ω ; the inductance of each coil is $190\mu\text{H}$, the total inductance is $380\mu\text{H}$. An elastic string is adopted in the presented study not only because it difficulty to find a suitable metal spring with the desired stiffness, but also because it will not generate counter-acting force when $l < l_0$. The disadvantage of the elastic string is that its stiffness is not constant. It varying with the extension state which will make the resonant frequency variation range more bigger. The efficiency of elastic string is also usually lower than a metal spring which means more energy will be dissipated by string.

The generated energy is harvested by chip of LTC[®]3109 which is a highly integrated DC/DC converter ideal for harvesting low input voltage sources [35]. The allowed input voltage range of LTC[®]3109 is $\pm 30\text{mV}$ to $\pm 500\text{mV}$. The energy manage circuit is shown in Fig. 13. All the experiment results are sampled by a digital oscilloscope (YOKOGAWA DL9510L).

4.2. Resonant frequency test

The resonant frequency of the generator is tested by an impulse motion of the container. Two initial extension states are tested for comparison and two directions are tested independently. The measured state is the open-circuit generated voltage of the coil. The results of X-direction and Y-direction test are illustrated in the Fig. 14a and 14b, respectively. The results in

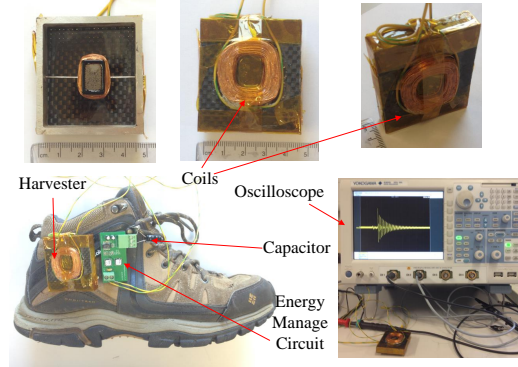


Figure 12: Prototype of proposed energy harvester

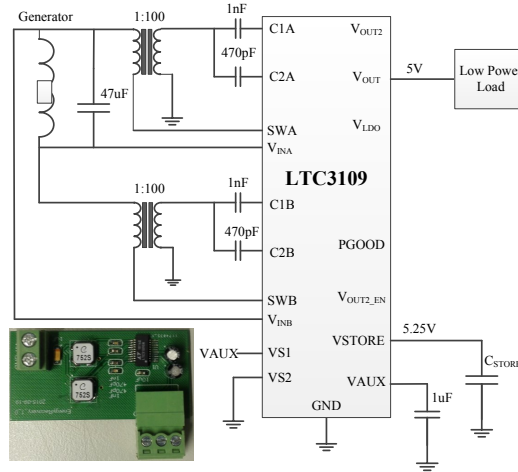


Figure 13: Energy manage circuit schematic and prototype photograph

274 Fig. 14a indicate that there are two main resonant frequencies. The resonant
 275 frequency in the X -direction which is the lower one is about 8Hz in the loose
 276 string condition ($l_0 = 13\text{mm}$) and about 12Hz in the tight condition ($l_0 =$
 277 8mm). The results in Fig. 14b indicate that there are three main resonant
 278 frequencies when impulse in Y direction. The resonant frequency in the Y -
 279 direction which is the middle one is about 12Hz in the loose string condition
 280 and about 16Hz in the tight condition. The third resonant frequency is on
 281 the rotary DoF. It also should be noticed that the resonant frequencies are
 282 not matching well in the X direction and Y direction impulse test. That
 283 can be because the stiffness is varying under different extension condition.
 284 In the X -direction test, the PM move farther than Y -direction test due to

the lower stiffness, therefore, the string extends longer, which makes the diameter of the string smaller in turns decreases the K_s . On contrary, in the Y -direction test, the PM move less distance which has higher K_s . Thus the resonant frequencies in Y -direction impulse test are higher. The third resonant frequency only appears in the Y -direction impulse test because it is difficult to be excited under X -direction impulse test.

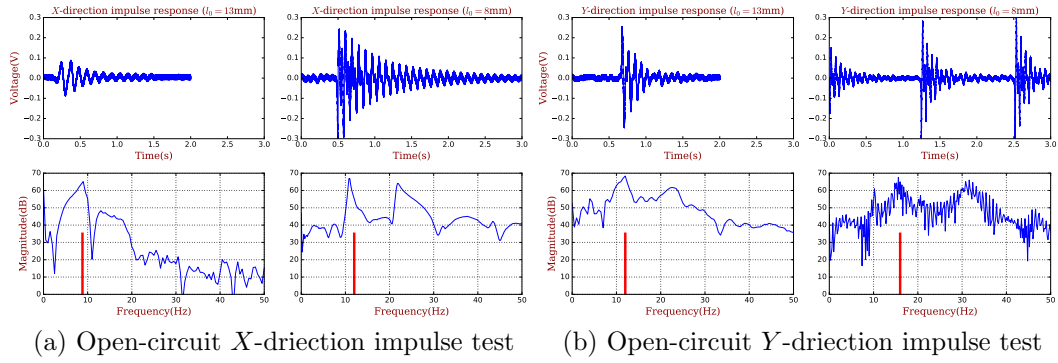


Figure 14: Open circuit impulse test

4.3. Resistance load test

A resistance load test is carried to measure how much electrical energy can be harvested by the proposed harvester. A 2Ω resistor is connected between two ends of the coil and the voltage at the resistor is measured. The results of walking and running is shown in Fig. 15a and Fig. 15b. The results of walking condition indicated that the tight one generate higher voltage and more energy because of the higher resonant frequency. The harvester can harvest 0.003J and 0.0052J at walking and running condition in 4s, respectively. It means the average powers of these two conditions are 0.75mW and 1.4mW. The results also indicate that although the major frequency of walking step is about 1Hz, the high frequency energy of the impulse of footfall can be absorbed by the harvester. High frequency vibration has more power which is benefit for enhancing the output power.

4.4. Energy storage test

The energy storage test which using the energy harvest circuit to change the generate voltage into 5VDC and store in a capacitor is carried to evaluate how much energy can be transfered and stored. A $1000\mu\text{F}$ capacitor is used

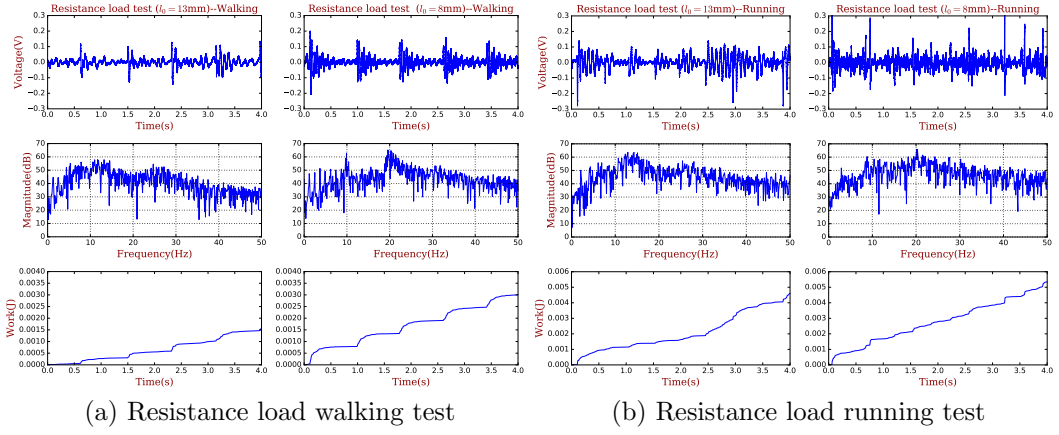


Figure 15: Resistance load test.

to store the DC energy. The voltage of the capacitor is measured. The results are shown in Fig. 16a and Fig. 16b. In the walking condition, the loose one make the voltage of capacitor from 0.62V to 0.85V in 10s, which can calculate that the average power is $16.9\mu\text{W}$, and the tight one make the voltage of capacitor from 0.46V to 0.89V, which can calculate that the average power is about $29.0\mu\text{W}$. In the running condition, the loose one make the voltage of capacitor from 0.42V to 0.77V in 10s, which can calculate that the average power is $20.8\mu\text{W}$, and the tight one make the voltage of capacitor from 0.4V to 0.93V, which can calculate that the average power is about $35.2\mu\text{W}$. Comparing the results of resistance load test and the energy storage test indicates that only 3% of energy is transferred and stored into the capacitor. The energy harvest circuit has a great potentiality to improve the transferring and storing efficiency.

5. Conclusions

The design, modeling, fabrication, and characterization of a human wearable electromagnetic resonant energy harvester were introduced and discussed in this paper. It utilized a PM connecting with two elastic strings as a 3-Dof resonator. The resonator was put into a rectangle box and two windings were placed on the surface of the box to compose the electromagnetic resonant energy harvester. The 3 Dof resonator can extract kinetic energy from all direction in the device plane as well as broaden the band-

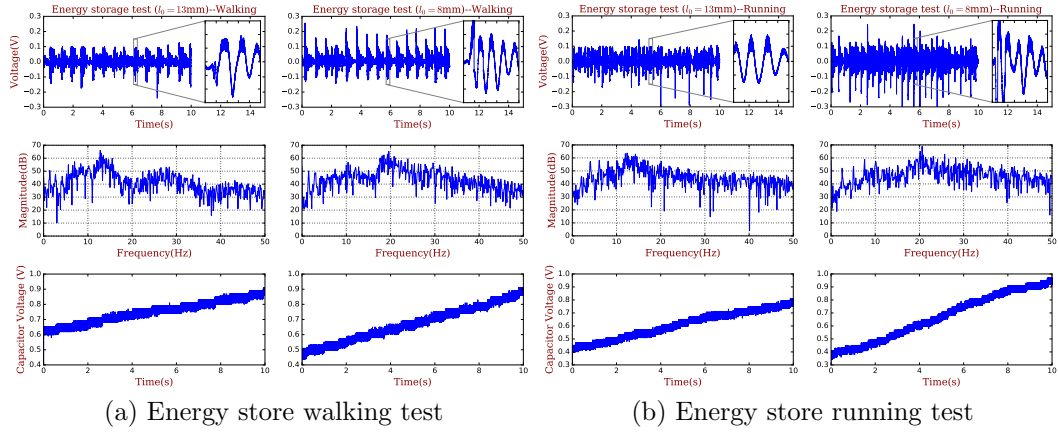


Figure 16: Energy storage test.

width, increase the efficiency of the energy. This harvester can wear on the shoe which can absorb the footfall energy. The structure and the stiffness were optimized to adjust the resonant frequency. It has three main resonant frequency which can absorb more frequency range kinetic energy. The Ferrofluid was adopted to decrease friction, which is one of the main challenge for improving efficiency of this type small energy harvester. The ferrofluid made the PM away from the plate of the box which decreased the friction significantly. The resistance load test results indicated the proposed harvester can reach the power level of 1.4mW when running. A energy storage circuit which can transfer the generated low voltage alternating current to 5V direct current was also developed. The energy storage test results indicated that the electrical storage power level was 35.2 μ W when running. The developed harvester can be used to offer continuous power supply for wearable sensor and device, such as activity trackers. Possible future research topic can be the improving storage efficiency and enhance the generate power to make it more practicable.

Acknowledgment

This study was co-supported by the National Key Basic Research and Development Program (Grant No. 2014CB046401) and the National Natural Science Foundation of China (Grant No. 51235002). This work is supported partially by Chinese Scholar Council, and by Cranfield University who is host

350 to the first author.

351 References

- 352 [1] Y. Qi, M. C. McAlpine, Nanotechnology-enabled flexible and biocom-
353 patible energy harvesting, *Energy & Environmental Science* 3 (9) (2010)
354 1275–1285.
- 355 [2] C.-Y. Sue, N.-C. Tsai, Human powered mems-based energy harvest de-
356 vices, *Applied Energy* 93 (2012) 390 – 403.
- 357 [3] T. Starner, Human-powered wearable computing, *IBM systems Journal*
358 35 (3.4) (1996) 618–629.
- 359 [4] J. Kyminsis, C. Kendall, J. Paradiso, N. Gershenfeld, Parasitic power
360 harvesting in shoes, in: *Wearable Computers, 1998. Digest of Papers.*
361 *Second International Symposium on*, IEEE, 1998, pp. 132–139.
- 362 [5] N. S. Shenck, J. A. Paradiso, Energy scavenging with shoe-mounted
363 piezoelectrics, *IEEE micro* (3) (2001) 30–42.
- 364 [6] W. Yang, J. Chen, G. Zhu, J. Yang, P. Bai, Y. Su, Q. Jing, X. Cao, Z. L.
365 Wang, Harvesting energy from the natural vibration of human walking,
366 *ACS Nano* 7 (12) (2013) 11317–11324.
- 367 [7] P. D. Mitcheson, E. M. Yeatman, G. K. Rao, A. S. Holmes, T. C. Green,
368 Energy harvesting from human and machine motion for wireless elec-
369 tronic devices, *Proceedings of the IEEE* 96 (9) (2008) 1457–1486.
- 370 [8] H. Vocca, I. Neri, F. Travasso, L. Gammaitoni, Kinetic energy harvest-
371 ing with bistable oscillators, *Applied Energy* 97 (2012) 771 – 776, *energy*
372 *Solutions for a Sustainable World - Proceedings of the Third Interna-*
373 *tional Conference on Applied Energy*, May 16-18, 2011 - Perugia, Italy.
- 374 [9] J. Zhao, Z. You, A shoe-embedded piezoelectric energy harvester for
375 wearable sensors, *Sensors* 14 (7) (2014) 12497–12510.
- 376 [10] S. Zhou, J. Cao, D. J. Inman, J. Lin, S. Liu, Z. Wang, Broadband
377 tristable energy harvester: Modeling and experiment verification, *Ap-*
378 *plied Energy* 133 (2014) 33 – 39.

- 379 [11] K. Pietrzyk, J. Soares, B. Ohara, H. Lee, Power generation modeling for
380 a wearable thermoelectric energy harvester with practical limitations,
381 Applied Energy 183 (2016) 218 – 228.
- 382 [12] Y. K. Ramadass, A. P. Chandrakasan, A batteryless thermoelectric
383 energy-harvesting interface circuit with 35mv startup voltage, Institute
384 of Electrical and Electronics Engineers, 2010.
- 385 [13] Y. Yang, H. Zhang, Z.-H. Lin, Y. S. Zhou, Q. Jing, Y. Su, J. Yang,
386 J. Chen, C. Hu, Z. L. Wang, Human skin based triboelectric nanogener-
387 ators for harvesting biomechanical energy and as self-powered active
388 tactile sensor system, ACS Nano 7 (10) (2013) 9213–9222.
- 389 [14] R. D. Kornbluh, R. Pelrine, Q. Pei, R. Heydt, S. Stanford, S. Oh, J. Eck-
390 erle, Electroelastomers: applications of dielectric elastomer transducers
391 for actuation, generation, and smart structures, in: SPIE’s 9th Annual
392 International Symposium on Smart Structures and Materials, Interna-
393 tional Society for Optics and Photonics, 2002, pp. 254–270.
- 394 [15] A. Bibo, R. Masana, A. King, G. Li, M. Daqaq, Electromagnetic
395 ferrofluid-based energy harvester, Physics Letters A 376 (32) (2012)
396 2163–2166.
- 397 [16] P. Patel, Development of electromagnetic micro-energy harvesting de-
398 vice, Ph.D. thesis, University of Waterloo, Waterloo, Ontario, Canada
399 (7 2013).
- 400 [17] Y. Wang, Q. Zhang, L. Zhao, E. S. Kim, Ferrofluid liquid spring for
401 vibration energy harvesting, in: Micro Electro Mechanical Systems
402 (MEMS), 2015 28th IEEE International Conference on, IEEE, 2015,
403 pp. 122–125.
- 404 [18] R. Torah, P. Glynne-Jones, M. Tudor, T. O’Donnell, S. Roy, S. Beeby,
405 Self-powered autonomous wireless sensor node using vibration energy
406 harvesting, Measurement science and technology 19 (12) (2008) 125202.
- 407 [19] R. Gherca, R. Olaru, Harvesting vibration energy by electromagnetic
408 induction, Annals of the University of Craiova.

- 409 [20] A. R. M. Foisal, G.-S. Chung, Design and analysis of a vibration-driven
410 aa size electromagnetic energy harvester using magnetic spring, *Trans-*
411 *actions on Electrical and Electronic Materials* 13 (3) (2012) 125–128.
- 412 [21] B. Yang, C. Lee, W. Xiang, J. Xie, J. H. He, R. K. Kotlanka, S. P.
413 Low, H. Feng, Electromagnetic energy harvesting from vibrations of
414 multiple frequencies, *Journal of Micromechanics and Microengineering*
415 19 (3) (2009) 035001.
- 416 [22] B. J. Bowers, D. P. Arnold, Spherical, rolling magnet generators for pas-
417 sive energy harvesting from human motion, *Journal of Micromechanics*
418 *and Microengineering* 19 (9) (2009) 094008.
- 419 [23] N. Fondevilla, C. Serre, M. Acero, E. Cabruja, H. Campanella, J. Es-
420 teve, et al., Electromagnetic harvester device for scavenging ambient me-
421 chanical energy with slow, variable, and randomness nature, in: *Power*
422 *Engineering, Energy and Electrical Drives (POWERENG)*, 2011 Inter-
423 national Conference on, IEEE, 2011, pp. 1–5.
- 424 [24] M. Gorlatova, J. Sarik, G. Grebla, M. Cong, I. Kymissis, G. Zussman,
425 Movers and shakers: Kinetic energy harvesting for the internet of things,
426 *Selected Areas in Communications, IEEE Journal on* 33 (8) (2015) 1624–
427 1639.
- 428 [25] G. V. Merrett, H. Huang, N. M. White, Modeling the effect of orienta-
429 tion on human-powered inertial energy harvesters, *IEEE Sensors Journal*
430 15 (1) (2015) 434–441.
- 431 [26] S. Chae, S. Ju, Y. Choi, S. Jun, S. Park, S. Lee, H. Lee, C. Ji, Elec-
432 tromagnetic vibration energy harvester using springless proof mass and
433 ferrofluid as a lubricant, in: *Journal of Physics: Conference Series*, Vol.
434 476, IOP Publishing, 2013, p. 012013.
- 435 [27] C. Rinaldi, A. Chaves, S. Elborai, X. T. He, M. Zahn, Magnetic fluid
436 rheology and flows, *Current Opinion in Colloid & Interface Science* 10 (3)
437 (2005) 141–157.
- 438 [28] S. Van Veen, Planar ferrofluid bearings for precision stages, Ph.D. thesis,
439 TU Delft, Delft University of Technology (2013).
- 440 [29] COMSOL, Inc., Nonlinear Ferrohydrodynamics of Magnetic Fluids.

- 441 [30] Ferrotec (USA) Corporation, 33 Constitution Drive, Bedford, N.H.
442 03110, MATERIAL SAFETY DATA SHEET- EFH Series (3 2009).
443 URL <https://www.ferrotec.com/downloads/efhmsds.pdf>
- 444 [31] H. R. Yun, D. J. Lee, J. R. Youn, Y. S. Song, Ferrohydrodynamic energy
445 harvesting based on air droplet movement, *Nano Energy* 11 (2015) 171–
446 178.
- 447 [32] S. Odenbach, *Ferrofluids: magnetically controllable fluids and their ap-*
448 *plications*, Vol. 594, Springer, 2008.
- 449 [33] R. Ravaud, G. Lemarquand, Design of ironless loudspeakers with fer-
450 rofluid seals: Analytical study based on the coulombian model, *Progress*
451 *in Electromagnetics research B* 14 (2009) 285–309.
- 452 [34] R. Ravaud, G. Lemarquand, V. Lemarquand, Mechanical properties of
453 ferrofluid applications: centering effect and capacity of a seal, *Tribology*
454 *International* 43 (1) (2010) 76–82.
- 455 [35] D. Lee, Energy harvesting chip and the chip based power supply devel-
456 opment for a wireless sensor network, *Sensors* 8 (12) (2008) 7690–7714.

An electromagnetic wearable 3-DoF resonance human body motion energy harvester using ferrofluid as a lubricant

Wu, Shuai

2017-04-22

Attribution-NonCommercial-NoDerivatives 4.0 International

Wu S, Luk P, Li C, Zhao X, Jiao Z, Shang Y. (2017) resonance human body motion energy harvester using ferrofluid as a lubricant, Applied Energy, Volume 197, July 2017, pp. 364-374
<http://dx.doi.org/10.1016/j.apenergy.2017.04.006>

Downloaded from CERES Research Repository, Cranfield University